Optik 124 (2013) 7075–7079

Contents lists available at ScienceDirect

Optik

journal homepage: www.elsevier.de/ijleo

Comparative analysis for measurement precision of phase retrieval wavefront sensor

Xinxue Ma[a,b], Jianli Wang[a,*], Bin Wang[a], Hongzhuang Li[a], Yuanhao Wu[a], Zongyang Wang[a], Peifeng Wei[a]

[a] Changchun Institute of Optics, Fine Mechanics and Physics, Chinese Academy of Sciences, Changchun 130033, China
[b] University of Chinese Academy of Sciences, Beijing 100039, China

ARTICLE INFO

Article history:
Received 24 January 2013
Accepted 29 May 2013

Keywords:
Phase retrieval
Wavefront sensor
ZYGO interferometer
Liquid crystal space light modulator
Zernike

ABSTRACT

In order to analyze the performance of phase retrieval wavefront sensor (PRWS), an experimental based on the PRWS method has been built. In this paper, we utilize liquid crystal space light modulator (LC-SLM) to produce single aberration and random aberration, and validate the ability of PRWS measurement for any aberrations. Mathematic model of phase retrieval measurement is constructed based on the diffraction theory, and solved using gradient based optimization algorithm. Experimental results demonstrate that good agreement is obtained among the errors distribution, PV value and RMS value of ZYGO interferometer. The measurement precision of wavefront is 3/1000 wavelength RMS. Therefore, the feasibility and accuracy of the proposed method can be confirmed.

1. Introduction

Dynamic detection of the mirror surface in the optical processing of the reign of real-time detection and optical system alignment and the use of medium wave aberration of the process is difficult to complete traditional optical inspection equipment [1–3]. PRWS technology [4–8] based on the focal plane image information wavefront solver in the focal plane wavefront detection technology, whose principle is given by sampling a number of the defocus images [9–14]; solve the optical system wavefront by Fourier optical methods. System hardware is simple, free from the environment (especially the vibration) influence of optical components and systems for dynamic detection [7,15], real-time display of measurements, which has good application prospects in the field of the optical processing, system alignment, active optics, adapt optics, etc.

This paper, introduces the principle of PRWS, builds the experimental of the measurement method based on PRWS, and uses a LC-SLM produce single and random aberration to verify the detection capabilities of various aberrations of PRWS. Comparing the PRWS measurement result with ZYGO interferometer [16–21] measurement result, we can see that in the face shape error distribution, erroneous peak valley value (*PV*) and on root-mean-square value (*RMS*), all of them have a high degree of consistency. Wavefront measurement accuracy achieves about 3/1000 wavelength *RMS*; it illustrates that the feasibility and the accuracy of the measurement method of PR, which provides a data basis for the subsequent study on the detection system based on PRWS. This paper is organized as follows: the theory of PRWS is presented in Section 2, the measurement experiment of comparing PRWS and ZYGO interferometer in Section 3 and the summary in Section 4.

2. The principles of PRWS

Phase retrieval (PR) system is the wavefront detector of a focal plane waves; a laser spot light on the object plane is a target designated from the focal plane image acquisition, use the acquired image, the defocus of the corresponding image, known pupil size and shape to reverse solve the aberration of the optical system [22]. The structure of the PR system is shown in Fig. 1.

Assuming that the aperture of a measured optical system is D, the focal length is Z, the center wavelength of the laser light source is λ, whose pupil constraint function is $|f(x)|$, the generalized pupil function for focus plane is

$$f(x) = |f(x)| \exp[i\theta(x)] \tag{1}$$

where θ is wavefront distortion and can be obtained with Zernike polynomial fitting: $\theta(x) = \sum_n \alpha_n Z_n(x)$, the real number α_n

* Corresponding author.
E-mail address: eatingbeen@hotmail.com (J. Wang).

0030-4026/$ – see front matter © 2013 Elsevier GmbH. All rights reserved.
http://dx.doi.org/10.1016/j.ijleo.2013.05.143

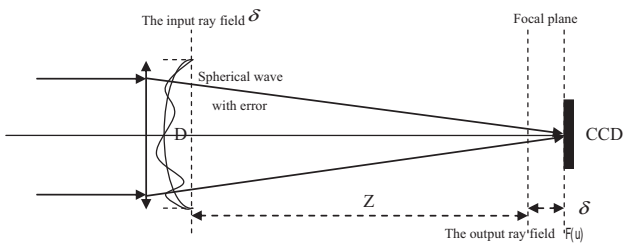

Fig. 1. Schematic of optical path of PR.

represents the first nth terms of polynomial coefficients, Z_n indicates the first nth terms of Zernike polynomials basement.

For linear optical system, when the generalized pupil $f(x)$ whose defocus is δ in the plane, the impulse response function $F(u)$ is

$$F(u) = |F(u)| \exp[i\psi(u)] = \mathcal{F}\{f(x)\exp[\varepsilon(x,\delta)]\} \tag{2}$$

where x is the coordinates of the pupil domain, u is the coordinates of the image domain, both of them are two-dimensional vector field coordinates. ψ is the phase part of the impulse response, $\mathcal{F}$ is two-dimensional Fourier transform, $\varepsilon(x,\delta)$ is wavefront aberration caused by defocus δ in the position x.

For a PR system, $|f(x)|$ of Eq. (1) is the priori conditions of a known optical system, corresponds to the size and shape of the pupil. $|f(u)|^2$ is the image collected by *CCD* where the defocus is δ. Therefore, the purpose that we detect wavefront by PR is to get α_n by the above known quantity. So formal description of the problem for: $|f(x)|$, δ_1, $|F_1(u)|^2$, δ_2, $|F_2(u)|^2$, ..., $|F_M(u)|^2$ are known. Image acquisition distance from the focal plane at $\delta_1, \delta_2, \ldots, \delta_M$ respectively is $|F_1(u)|^2$, $|F_2(u)|^2$, ..., $|F_M(u)|^2$.

The objective function and the partial derivative of PR objective function with respect to α_n respectively is formulae (3) and (4)

$$B_k = E_{Fk}^2 = N^{-2}\sum_{m=1}^{M}\sum_{u}[|G_{m,k}(u)| - |F(u)|]^2 \tag{3}$$

$$\partial_{a_n} B_k = -2\sum_{m}\sum_{x}|f(x)||g'_{m,k}(x)|\sin[\theta'_{m,k}(x) - \theta_{m,k}(x)]Z_n(x) \tag{4}$$

According to the objective function (3) and derivative (4) solve the wavefront, so we need to use the optimization algorithm, here we use LBFGS algorithm that the phase diversity (PD) [23–26] experiment has been able to solve.

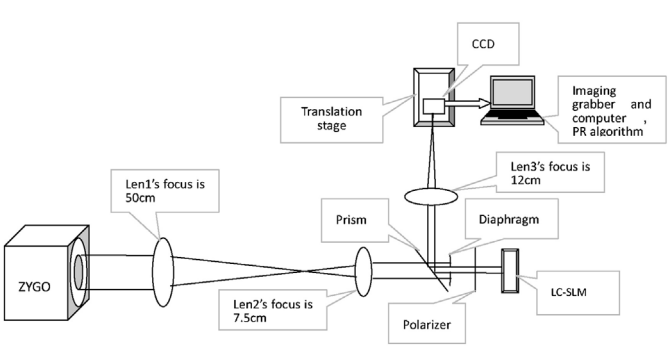

Fig. 2. Schematic diagram of PRWS.

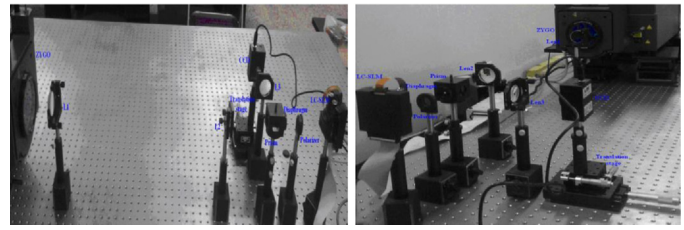

Fig. 3. The experimental system.

3. The contrast detection experiments between PRWS measurements and the interferometer

3.1. Experimental theory and components

The schematic diagram of PRWS is shown in Fig. 2. The parallel light from ZYGO interferometer pass through the $L1$ and $L2$ shrink beam group, after the beam splitter, one of which get into the aperture diaphragm, and then through a polarizer, incident to the liquid crystal spatial light modulator (LC-SLM) [27–29].

Since the effective area of the LC-SLM is only 6.14 mm × 6.14 mm, with light bar to limit the aperture; In addition, the LC-SLM requirements of the incident linearly polarized light, so join the polarizer so that the beam through the partial direction coincide with the LC-SLM fast-axis. Through the control of the LC-SLM, the reflected beam with a specified phase information (aberration), pass through the polarizer and the light bar, again divides into two path by the beam splitter, one of which back through ZYGO interferometer, with which and the front-end flat reference mirror of the interferometer is reflected back the reference beam interfere form interference fringes. By analyzing the interference fringes, we can calculate detecting wavefront of loading on the LC-SLM. Another part passes through the convergent lens $L3$ assemble on the CCD camera, which is placed on a movable platform, move along the optical axis and the angle of the camera posture fine-tuning to get the focus before and after receiving a different amount of defocus images, we can obtain wavefront loaded by LC-SLM with the PR algorithm. Compare the two measurements.

The experimental optical path is shown in Fig. 3 focal length of $L3$ in the experimental system is 0.12 m, and the center wavelength is 632.5 nm, the exit pupil caliber is 0.005 m, depth of focus is about 0.73 mm. In the experiment, the defocus we select is 0 mm and 4.65 mm respectively, the corresponding defocus phase's *PV* is 0λ and 1.6λ. Camera pixel size is 6.45 μm, each defocus position respectively intercept 128 × 128 pixel size of target region, the exposure time is 20 ms, the accuracy of mobile platform is ±5 μm.

3.2. Experimental procedures

Step 1: Build the experimental system, start LC-SLM, and make it a flattened state, which does not produce the wavefront aberration, adjust the optical path, and try to adjust the small optical aberrations;
Step 2: To adjust the size and position of diaphragm, so that try to make the incident spot cut the inside effective area of the LC-SLM;
Step 3: Rotate polarizer makes polarizer through partial direction coincide with the fast axis of LC-SLM who plays the role of the phase modulation;
Step 4: Observe the fringes of ZYGO interferometer, and fine-tuned through the partial direction of the polarizer, making the contrast of the interference fringes largest;
Step 5: Adjust the translation stage until the points of light into the *CCD* get minimum, record the location, which as the position that the defocus is 0;

Step 6: Set the LC-SLM for the flattened state, and utilizes ZYGO interferometer measure; make the measured wavefront as *W*0 and as the reference wavefront of ZYGO interferometer in later experiments. Using *CCD* camera to collect image in the location that defocus distance is 0 mm and 4.65 mm and PRWS calculate wave front *W*1, which as the reference wave front of PRWS wave front in later experiments;
Step 7: Put a specified wave front distortion input to the LC-SLM, use ZYGO interferometer measure the wave front at this time, subtract the reference wave front *W*0 of ZYGO interferometer and the first four of Zernike coefficient, we can obtain wavefront measured by ZYGO that LC-SLM newly added;
Step 8: Adjust PRWS optical path, utilize the *CCD* camera gathering image in the place of defocus distance of 0 mm and 4.65 mm respectively, which as the input of PRWS and calculate wave front by PR algorithm, and then subtract the reference wave front *W*1 of PRWS and subtract the first four Zernike coefficient, we can obtain the new loaded wave front of LC-SLM by PRWS measured. Compare the measurements between ZYGO interferometer and PRWS.

3.3. Experimental results and discussion

We separately add single and random aberrations on LC-SLM, and compare the measurement between ZYGO interferometer and PRWS, as shown in Figs. 4–11. The aberration of the figures is wavefront minus the piston, tilt and defocus and so on introduced from system alignment.

We put the above two wave fronts separately as the reference wave front of ZYGO interferometer and PR in later measurement.

Table 1 gives the contrast of *RMS* on the different aberration measurements of PRWS and ZYGO interferometer. We obtain measurement results for single aberration of Zernike as well as random aberrations, where we only enumerate a number of aberrations compared results, from which we can see that the peak and valley in the distribution of the surface error and the error value *PV* and *RMS* value, they have a high degree of consistency, measurement accuracy reach 3/1000λ *RMS*, which shows that the feasibility and accuracy of the measurement method by PRWS. In order to illustrate the accuracy of PRWS from another angle, we load the LC-SLM random aberration like Fig. 6, then collect the images in the location of the defocus distance is −4.5 mm, −3 mm, 0 mm, 3 mm, 4.5 mm

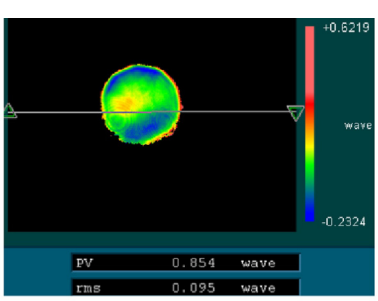

(a) Result of ZYGO interferometer measurement

RMS = 0.095λ , PV = 0.854λ

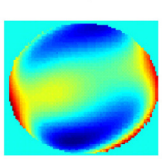

(b) Result of PR measurement, RMS = 0.046λ , PV = 0.246λ

Fig. 4. Contrast measurements when LC-SLM unfolds.

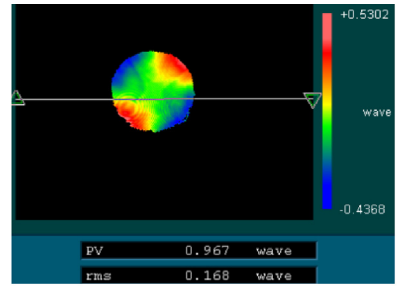

(a) Result of ZYGO interferometer measurement

$RMS = 0.168\lambda$, $PV = 0.967\lambda$

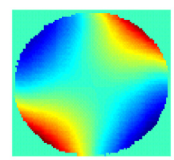

(b) Result of PR measurement, RMS =0.171λ, PV =0.893λ

Fig. 5. Contrast measurements when LC-SLM by adding astigmatic.

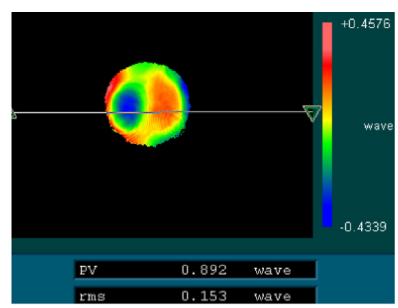

(a) Result of ZYGO interferometer measurement

RMS =0.153λ, PV =0.892λ

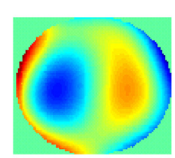

(b) Result of PR measurement, RMS =0.152λ, PV =0.928λ

Fig. 6. Contrast measurements when LC-SLM adds coma.

with the *CCD* image, as shown in Fig. 12. Then solves the point spread function of above six positions, as shown in Fig. 13 with the wavefront that PRWS measured as shown in Fig. 6(b).

It can be from Figs. 12 and 13, collected and calculated image have a great deal of similarity, which illuminate the accuracy of PRWS.

From the above experimental results, it can be seen that PRWS has very high detection accuracy to meet the actual needs of the project and has many advantages which ZYGO interference does not have:

1. There is little affection of the platform on PRWS, and even can be ignored.

Table 1
PRWS and ZYGO interferometer on the *RMS* contrast of the different aberration measurements.

	Astigmatism	Coma	Trefoil	Tertiary coma	Tetrafoil	Secondary spherical	Tertiary astigmatism
PR	0.171λ	0.152λ	0.144λ	0.148λ	0.109λ	0.197λ	0.148λ
ZYGO	0.168λ	0.153λ	0.147λ	0.148λ	0.109λ	0.199λ	0.152λ

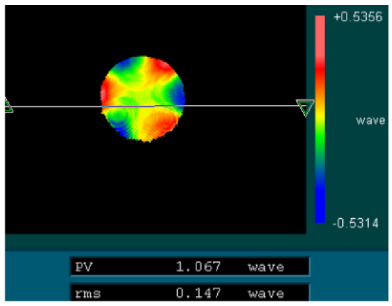

(a) Result of ZYGO interferometer measurement

RMS =0.147λ, PV =1.067λ

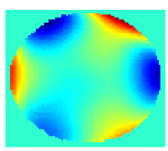

(b) Result of PR measurement, RMS =0.144λ , PV =1.011λ

Fig. 7. Contrast measurements when LC-SLM adds trefoil.

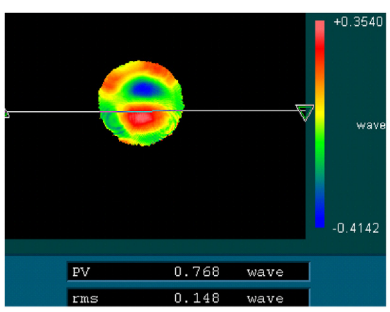

(a) Result of ZYGO interferometer measurement

RMS =0.148λ, PV=0.768λ

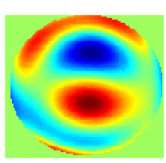

(b) Result of PR measurement, RMS =0.148λ, PV =0.705λ

Fig. 8. Contrast measurements when LC-SLM loads the tertiary coma.

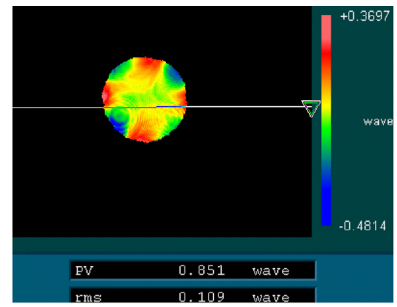

(a) Result of ZYGO interferometer measurement

RMS =0.109λ, PV =0.851λ

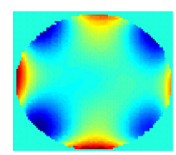

(b) Result of PR measurement, RMS = 0.109λ , PV = 0.732λ

Fig. 9. Contrast measurements when LC-SLM adds tetrafoil.

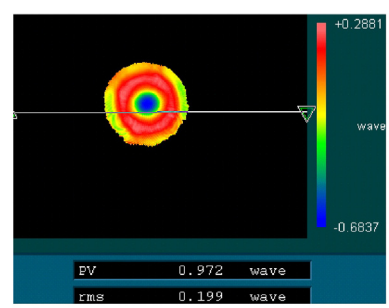

(a) Result of ZYGO interferometer measurement

RMS =0.199λ, PV =0.972λ

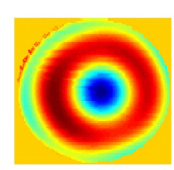

(b) Result of PR measurement, RMS =0.197λ, PV =0.943λ

Fig. 10. Contrast measurements when LC-SLM adds the secondary spherical.

2. The PRWS structure is simple, even use the camera which the imaging system has to detect the whole optical system under the conditions that without changing anything;
3. *CCD* of PRWS only with fewer sampling points can get a high measurement accuracy, as shown in Fig. 12, although we intercept the image is 128 × 128, the actual useful pixel area is only in 40 × 40, as shown in Fig. 2. If we do not join the *L*1 and *L*2 to extend the beam, but use ZYGO interferometer to measure the LC-SLM active area 6.14 mm × 6.14 mm directly, we will not detect the wave front due to ZYGO interferometer sampling insufficiency, which is we found in the pre-constructed optical path of experiment.

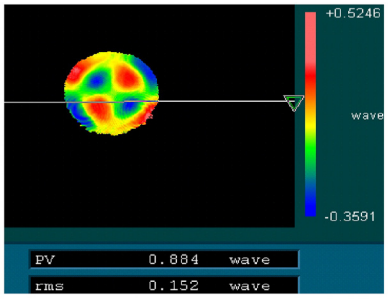

(a) Result of ZYGO interferometer measurement

RMS = 0.152λ , PV = 0.884λ

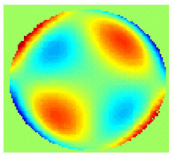

(b) Result of PR measurement, RMS = 0.148λ , PV =1.005λ

Fig. 11. Contrast measurements when LC-SLM adds the tertiary astigmatism.

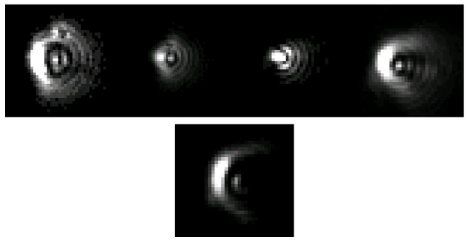

Fig. 12. Acquired images.

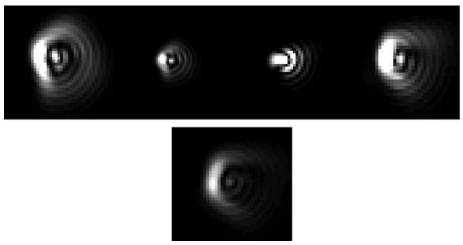

Fig. 13. Calculated by the images.

4. Conclusions

This paper has built the experimental platform using PRWS and ZYGO interferometer to measure different wave front aberrations and compared the measurement results; we quantitatively analyzed the accuracy of PRWS wave front measurement. During the experiment, we fully appreciate the ability of PRWS anti-vibration comparing to ZYGO interferometer, the optical path is simple, we have obtained a merit that we exactly solved the wavefront with fewer camera sampling point, which provides the feasibility to data support for our later search for online detection of the large mirror surface.

Acknowledgment

This work is supported by the National High-tech Research and Development Program (863 Program) (No. 2009AA8080603).

References

[1] G.R. Brady, J.R. Fienup, Improved optical metrology using phase retrieval, in: Optical Fabrication & Testing, 10, Rochester, NY, 2004, pp. 1–3.
[2] Y. Wu, X. Hu, Y. Dai, et al., Research on In-situ surface measurement for large aperture optical mirror based on phase retrieval technology, J. Chin. J. Mech. Eng. 45 (2) (2009) 157–163.
[3] W. Osten, Some answers to new challenges in optical metrology, in: Proc. SPIE, 7155, 2008, pp. 715503-1–715503-16.
[4] C.M. Ohara, J.A. Faust, A.E. Lowman, et al., Phase retrieval camera optical testing of the advanced mirror system demonstrator, in: SPIE, 5487, 2004, pp. 1744–1756.
[5] R.W. Gerchberg, W.O. Saxton, A practical algorithm for the determination of phase from image and diffraction phase pictures, J. Opt. 35 (2) (1972) 237–246.
[6] J.R. Fienup, Phase retrieval algorithms: a comparison, J. Appl. Opt. 21 (15) (1982) 2758–2769.
[7] J.R. Fienup, J.C. Marron, T.J. Schulz, et al., Hubble space telescope characterized by using phase-retrieval algorithms, J. Appl. Opt. 32 (10) (1993) 1747–1767.
[8] H. Dean Bruce, L. Aronstein David, J.S. Smith, et al., Phase retrieval algorithm for JWST flight and testbed telescope, in: Proc. of SPIE, 6265, 2006, pp. 1–17.
[9] F. Zeng, Q. Tan, X. Wei, et al., A phase retrieval algorithm for complex optical field, J. Chin. J. Lasers 33 (3) (2006) 339–342.
[10] X. Deng, F. Gao, C. Liu, et al., Non-paraxial approximation of scalar diffraction theory and its validity, J. Acta Photonica Sin. 35 (6) (2006) 898–901.
[11] B. Yu, X. Peng, J. Tian, et al., Phase retrieval for in-line hard X-ray phase-contrast imaging with the Yang-Gu algorithm, in: Proc. of SPIE, 6026, 2006, pp. 60260Z.1–60260Z.6.
[12] N. Wang, T. Zhang, H. Hong, et al., Restoration of turbulence-degraded images based on phase retrieval algorithm, J. Infrared Laser Eng. 34 (5) (2005) 597–601.
[13] B. Yu, X. Peng, J. Tian, et al., Phase retrieval for hard X-ray in-line phase contrast imaging, J. Acta Phys. Sin. 54 (5) (2005) 2034–2037.
[14] A.J. Devaney, R. Childlaw, On the uniqueness question in the problem of phase retrieval from intensity measurement, J. JOSA A 68 (10) (1978) 1352–1354.
[15] R. Brady Gregory, J.R. Fienup, Phase retrieval as an optical metrology tool, in: Optical Fabrication & Testing. Topical Meeting of the Optical Society of America, SPIE Technical Digest TD03, 2005, pp. 139–141.
[16] J.E. Millerd, J.C. Wyant, Simultaneous phase-shifting Fizeau interferometer, US Patent 20,050,046,864 (2005).
[17] L. Deck, Vibration-resistant phase-shifting interferometry, J. Appl. Opt. 35 (34) (1996) 6655–6662.
[18] J.H. Burge, J.C. Wyant, Applications of computer-generated holograms for interferometric measurement of large aspheric optics, in: Proc. SPIE, 2576, 1995, pp. 258–269.
[19] S. Reichelt, C. Pruss, H.J. Tiziani, Absolute interferometric test of aspheres by use of twin computer-generated holograms, J. Appl. Opt. 42 (22) (2003) 4468–4479.
[20] G.E. Sommargren, D.W. Phillion, E.W. Campbell, Sub-nanometer interferometry for aspheric mirror fabrication, in: The 9th International Conference on Production Engineering, Osaka, Japan, 1999.
[21] S. Reichelt, H.J. Tiziani, Twin-CGHs for absolute calibration in wavefront testing interferometry, J. Opt. Commun. 220 (2003) 23–32.
[22] M.A. Xinxue, W.A.N.G. Jianli, W.A.N.G. Bin, Study on phase retrieval algorithm, J. Laser Infrared 42 (2) (2012) 217–221.
[23] Y.H. Wu, B. Wang, J.Y. Zhao, et al., Restoration of broadband white light image using phase diversity technique, J. Opt. Precision Eng. 18 (8) (2010) 1849–1854.
[24] J.L. Wang, Z.Y. Wang, B. Wang, et al., Image restoration by Phase-diversity Speckle, J. Opt. Precision Eng. 19 (5) (2011) 1165–1170.
[25] J.Y. Zhao, Z.F. Chen, B. Wang, et al., Improvement of phase diversity object function's parallelity, J. Opt. Precision Eng. 20 (2) (2012) 431–438.
[26] B. Wang, Z.Y. Wang, J.L. Wang, et al., Phase-diverse speckle imaging with two cameras, J. Opt. Precision Eng. 19 (6) (2011) 1384–1390.
[27] R.J. Noll, Zernike polynomials and atmospheric turbulence, J. Opt. Soc. Am. 66 (3) (1976) 207–211.
[28] N. Roddier, Atmospheric wavefirst simulation using Zernike polynomials, J. Opt. Eng. 29 (10) (1995) 1174–1180.
[29] D. Cai, N. Ling, W. Jiang, The performance of phase-only liquid crystal spatial light modulator used for generating Zernike terms, J. Acta Phys. Sin. (2008) 897–903.